

Search for cosmic-ray magnetic monopoles using a three-loop superconductive detector

R. D. Gardner, B. Cabrera, M. E. Huber,* and M. A. Taber
Physics Department, Stanford University, Stanford, California 94305

(Received 29 May 1990)

Superconducting detectors are ideal for the search for magnetic monopoles since their sensitivity is calculated from classical properties and is independent of the particle's mass, velocity, electric charge, or magnetic dipole moment. We describe the design and the completed operation of a superconducting three-loop inductive detector to search for magnetic monopoles in cosmic rays. The three-loop detector, with a total sensing area of 476 cm^2 averaged over $4\pi \text{ sr}$, was in operation for 1008 days. During that time, the detector logged 24 190 h of active operation. These data set an upper limit of $4.4 \times 10^{-12} \text{ cm}^{-2} \text{ s}^{-1} \text{ sr}^{-1}$ at 90% C.L. $(2.3/\int dA d\Omega dt)$ on any uniform flux of magnetically charged particles of any mass passing through the Earth's surface at any velocity.

I. INTRODUCTION

Theoretical interest in magnetic monopoles began in 1931 when Dirac [1] demonstrated that the existence of monopoles would be a sufficient condition to explain the quantization of electric charge. More recently, 't Hooft [2] and Polyakov [3] have shown that all grand unification theories predict the existence of stable magnetic monopoles with the Dirac value of magnetic charge $g_D = hc/4\pi e$ and a mass of $\approx 10^{16} \text{ GeV}/c^2$. Such massive particles could only have been created during the big bang and would now be moving slowly, at speeds $v/c \approx 10^{-3}$. Because they move so slowly and have no electric charge, they would be only weakly ionizing and highly penetrating. They could thus pass through the Earth and are difficult to observe with conventional particle detectors. Magnetic-induction techniques such as described here provide a means of detecting monopoles independently of their mass and velocity.

Before describing the operation of our three-loop detector in detail, we summarize some of the relevant astrophysical arguments on monopole abundance, conventional detection techniques, and the development of superconducting inductive detectors. We continue with a brief description of the interaction of a monopole with a superconducting loop, followed by a description of the physical apparatus. After describing the data-collection system, we conclude with a summary of the detector operation over a period of 3 years. For the interested reader, a thorough review of the particle theory of monopoles has been covered by Preskill [4]. Also, Groom [5] has prepared an excellent overview of the various theories of monopole abundance, along with a look at the techniques currently being used to search for them. These issues were also covered in detail at the Monopole '83 Conference [6,7] and the Conference on Magnetic Monopoles [8].

A. Astrophysical theories of abundance

Parker and collaborators [9–11] have suggested that the particle flux of magnetic monopoles is bounded from

above, based on the persistence of galactic magnetic fields (see Fig. 18). Since these fields would lose energy in the process of accelerating transient monopoles, a regeneration mechanism must be present if the fields are to persist. Comparing the loss of energy for a given particle flux to the known mechanisms for regeneration of galactic fields led Parker to propose an upper bound on the particle flux of magnetic monopoles of about $10^{-15} \text{ cm}^{-2} \text{ sr}^{-1} \text{ sec}^{-1}$. For a monopole mass above about $10^{17} \text{ GeV}/c^2$, the limit becomes less restrictive since the gravitational interaction with the galaxy becomes larger than the magnetic interaction. A further limit on the particle flux of monopoles arises from assuming that all of the "dark matter" in our galactic halo is provided by monopoles. There is compelling evidence that galaxies, including our own, are surrounded by massive halos of unknown matter which are observed only through their gravitational interaction with luminous objects. The galactic halo bound, however, becomes more restrictive than the Parker field-survival bound only for masses large enough to bind them to the galaxy, and the two bounds cross around $10^{19} \text{ GeV}/c^2$.

Arons and Blanford [12] derive a more optimistic flux limit by arguing that, if the monopole plasma oscillation frequency exceeds some lower bound, then the Parker analysis fails to account for the resonant character of the magnetic field damping. Since a large monopole plasma frequency ensures a high phase velocity and since high-phase-velocity components of the monopole's motion are negligibly damped, these oscillations would survive over time scales longer than the lifetime of the galaxy. They also argue that dynamo activity can regenerate the magnetic field in the presence of monopoles. The lower bound in this model is $\approx 10^{-12} \text{ cm}^{-2} \text{ sr}^{-1} \text{ sec}^{-1}$.

This argument was also studied in more detail by Shapiro and co-workers [13,14]. They point out that in the Parker-bound calculations a time-independent magnetic field is assumed, while the monopoles are treated dynamically. Instead, they self-consistently calculated the interaction between the galactic magnetic field and the monopole halo, using the generalized Faraday induction law

$$\nabla \times \mathbf{E} = -\frac{1}{c} \frac{\partial \mathbf{B}}{\partial t} - \frac{4\pi}{c} \mathbf{J}_m, \quad (1)$$

where J_m is the monopole current density. Their analytical and numerical results suggest that there can be little heating of the monopole halo on orbital time scales for self-consistent, time-dependent magnetic fields. The survival of large-scale galactic fields consequently implies that the monopole mass must be less than $\approx 10^{19}$ GeV/ c^2 , which gives a lower bound on the monopole flux of $\approx 10^{-13}$ cm $^{-2}$ sr $^{-1}$ sec $^{-1}$, assuming the galactic halo consists *entirely* of monopoles. The survival of smaller scale fluctuations (≈ 300 parsec) results in a lower bound of $\approx 10^{-11}$ cm $^{-2}$ sr $^{-1}$ sec $^{-1}$. It should be pointed out that these limits assume that the galactic halo is entirely monopoles. The limits must be lowered if monopoles make up only a fraction of the halo. Nonetheless, this self-consistent version of the Parker bound is far less restrictive than the conventional result.

A more restrictive bound results from the analysis of nucleon-decay catalysis models [15–17]. It has been found that grand unified theory monopoles can interact with ordinary matter in a way which does not conserve baryons. Therefore, if a magnetic monopole moves into the vicinity of a proton, it will cause the proton to decay rapidly; the monopole could then proceed to another nucleon and catalyze its decay. Bennett has shown [18], however, that the size of the decay cross section depends on the details of the particular grand unified theory and varies by several orders of magnitude. A number of monopole flux limits based on nucleon-decay catalysis can be calculated from observations of the luminosity of neutron stars and white dwarfs. If the larger cross sections are correct, nucleon-decay catalysis would provide a flux limit on monopoles that is five or six orders of magnitude smaller than the Parker bound and direct detection would be very difficult if not impossible.

B. Conventional detection techniques

Conventional particle detectors used in monopole searches can be made larger than superconducting inductive detectors. However, their predicted response is sensitive to models of the monopole interaction with matter. One way a slow-moving monopole can lose energy in matter is through adiabatic deformation of the electron cloud surrounding a nucleus (often referred to as the “Drell-Parke” mechanism). This has been studied by Drell and others [19–21] by calculating the adiabatic deformation of an atom with Z electrons as a monopole passes at an impact parameter b along a path parallel to the z axis. The atom can make a transition to an excited state with z component of angular momentum J_z increased by $Zh/4\pi$. A monopole changes the current in a conducting loop by essentially the same mechanism. The velocity threshold for the Drell-Parke effect is $(10^{-3}-10^{-4})c$. The energy level shift is found by superimposing solutions from the region where the monopole is far from the nucleus and from the region where the

monopole is at the nucleus. Improvements can be made by accounting for the separation of the monopole and the nucleus [20]. However, the mechanism fails entirely if a proton is bound to the monopole, a not-unlikely occurrence in the proton-rich intergalactic medium. One must thus determine the likelihood that a monopole will be free of any proton charge.

Proportional-wire-chamber (PWC) experiments based on the Drell-Parke mechanism can be used to establish a lower bound on the number flux of monopoles. However, while the effect should be observable in helium, it is not clear whether it will be observable in argon [5,21]. With the caveats discussed above, helium-based experiments have produced a lower limit of 10^{-13} cm $^{-2}$ sr $^{-1}$ sec $^{-1}$ with argon-based experiments giving a lower limit an order of magnitude smaller. Experiments now underway could lower this limit further [5].

C. Superconducting inductive detectors

A number of searches for magnetic monopoles have been carried out based on Faraday’s law of induction, which predicts that an emf exists in a closed conducting loop traversed by a magnetic monopole. This method is independent of monopole mass, velocity, or electric charge and is also model-independent (see the following section). It therefore provides the most convincing experimental bound on a monopole flux. If the conducting loop is superconducting, the current change can be persistent and detected with superconducting quantum interference device (SQUID) magnetometer techniques. Inductive detectors were suggested in 1963 by Alvarez [22] and independently by Tassie in 1964 [23], and were used by Eberhard *et al.* [24,25] and Ross *et al.* [26] to look for monopoles trapped in lunar ores. However, they did not have sufficient sensitivity to observe a monopole with a single pass through the detector.

In 1982, one of us (Cabrera [27]) reported a candidate event from a small single-loop superconductive detector in the first search for magnetically charged particles in cosmic rays. In an effort to increase the sensing area, we constructed the larger three-loop detector [28–31] described here with coincidence checking and other spurious event discrimination. This three-loop detector with an effective area of 485 cm 2 was in operation for 1008 days. We have since designed and constructed a larger eight-channel detector [32], which is described in the accompanying paper.

In addition to our group, there are now at least six other groups that have contributed to the search with superconducting inductive detectors [5].

(1) A group at IBM [33,34] pioneered the use of gradiometer loops to reduce sensitivity to vortex currents deposited in the magnetic shielding by the traversal of a magnetic monopole. They operated a six-gradiometer device with an effective area of 0.1 m 2 for 15 months starting in November 1983 [35]. They are currently operating a 1-m 2 detector in collaboration with Brookhaven National Laboratory [36].

(2) A collaboration between the University of Chicago,

Fermilab, and the University of Michigan [37–39] independently developed gradiometer structures. They also pioneered the use of distributed grids and parallel wiring of detector loops for impedance matching. They operated a 700-cm² detector for 8 months and then operated an 0.75-m² detector for several weeks.

(3) A group at Imperial College, London [40–42] used a detector with 17-cm-diameter coaxial loops and a large rectangular “window frame” loop with one side along the axis of the cylindrical shield and the other almost in contact with it. This detector has an effective area of 0.17 m², though the coincidence area of the detector is significantly smaller.

(4) A group at Kobe University used a detector to search for monopoles trapped in magnetic iron ores [43]. They heated magnetic iron ore above its Curie point over the detector to free any trapped monopoles from the ore. These monopoles would then fall through a superconducting loop under the influence of gravity.

(5) A group at Stony Brook [44] used a detector with two gradiometer loops in separate superconducting shields.

(6) A group at the National Bureau of Standards (NBS, now the National Institute of Standards and Technology, NIST) studied mechanisms for producing spurious events in a superconducting inductive detector by subjecting a small detector to mechanical shock, stress, and magnetic signals. They concluded that with adequate clamping and shielding such spurious signals could be avoided, and they have operated a three-loop detector similar to ours but slightly larger [45].

II. PRINCIPLE OF OPERATION

A monopole passing through a closed loop would change the flux through the loop by $4\pi g_D$, inducing a current of $4\pi g_D/L$, where L is the loop inductance. If the loop were composed of a normal metal, the induced current would quickly decay, making a dc measurement difficult. If, instead, the detector loop is superconducting, the current change is persistent (now permitting a dc measurement), and very sensitive SQUID magnetometers can be used to detect the small current changes. Since the flux quantum of superconductivity, $\Phi_0 = hc/2e$, is half that of the $4\pi g_D$ ($=hc/e$) magnetic flux threading the ring from the monopole, the passage of a magnetic monopole through a superconducting loop would change its quantum state by 2. The observance of flux quantization in a superconducting loop (readily measurable with SQUID technology) demonstrates that the loop has sufficient resolution to observe the passage of a magnetic monopole.

In this paper and the one that follows, we confine our discussion to the magnetic charge value g_D , or integer multiples of g_D , because, although classical Faraday induction [Eq. (1)] is valid for non-Dirac charges passing through a conducting ring, a superconducting ring would be left in a state inconsistent with flux quantization which stems from the macroscopic quantum nature of the superconducting state. This inconsistency would violate experimental evidence [46], and in fact, this inconsistency is

closely related to Dirac’s original argument for the quantization of electric and magnetic charges.

For practical detectors the induced current is on the order of nanoamps. A variation in the Earth’s magnetic field of 1 part in 10^8 would induce a similar current in our detector. Thus the detector must be shielded from external magnetic fluctuations, and the most effective shield is a superconducting shield. A monopole passing through the shield, however, will induce eddy currents in the shield at the penetration points. These currents contribute to the magnetic flux through the detector loop, usually reducing the current change in the loop. This effect must be included in calculating the detector response.

The time-dependent coupling of a monopole to a superconducting ring has been derived elsewhere [47]. One early concern was understanding the structure of the field lines as the monopole passes through the superconducting loop. On the one hand, the field lines must be brushed back since magnetic fields cannot penetrate a superconductor; on the other, all of the magnetic field lines emanating from the monopole cannot return through the loop as the monopole recedes to infinite distances. Figure 1 shows schematically the resolution of the problem—as field lines wrap around the loop, they eventually touch and separate.

Figure 2 shows a plot of the induced current in a superconducting loop from each of four separate trajectories that pass near or through the loop. For a superconducting loop of radius 4 cm and a monopole traveling at $v = 10^{-3}c$, the rise time is $\approx 10^{-7}$ sec. Trajectories

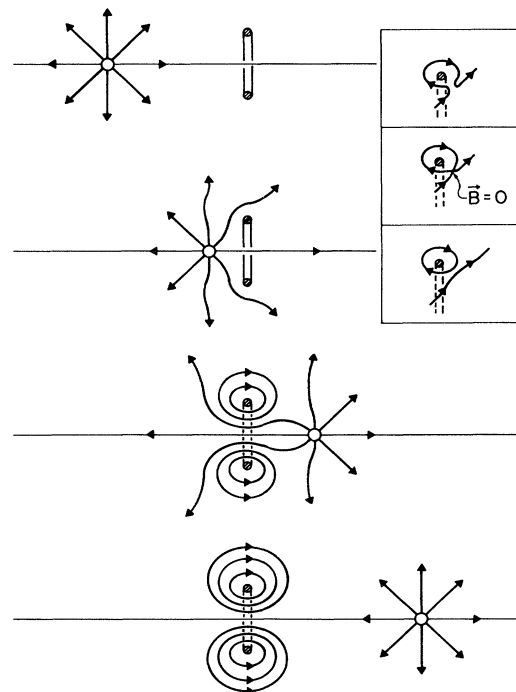


FIG. 1. Magnetic monopole passing through superconducting loop, showing how the magnetic field lines are bent and broken by the superconductor.

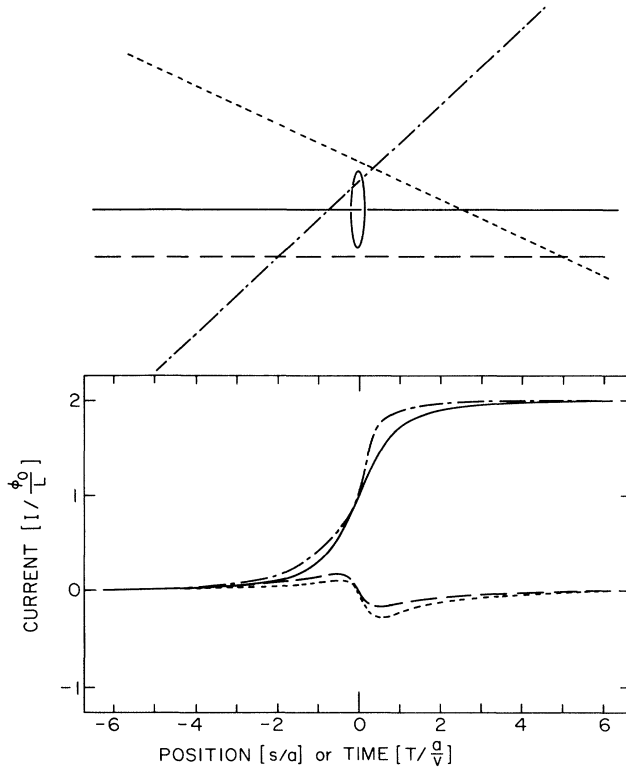


FIG. 2. Induced current I in a superconducting loop of radius a and inductance L for several monopole trajectories, both intersecting and missing the loop.

which miss the loop induce only transient currents with similar rise times and with a maximum peak-to-peak excursion of $1\Phi_0$. In an actual detector it is necessary to surround the loop with a superconducting shield to guard against magnetic-field changes. Currents induced in the shield by the passage of a monopole would also couple flux to the loops even if the trajectory of the monopole does not intersect the loop. We have not included this effect in the simple calculation above; however, we discuss it in detail below when calculating the response of the actual detector.

We thus see that as a magnetic monopole passes through a superconducting loop, it will change the number of flux quanta threading the loop by two. In addition, if it passes through a nearby bulk superconductor (such as a surrounding superconducting shield or the wire of the loop), it will create a doubly quantized vortex trapped in the bulk, changing the flux in the loop by some intermediate value.

A superconducting inductive detector is sensitive only to magnetic charge and the response is independent of electric charge, magnetic dipole, velocity, and mass. Its sensitivity is based on fundamental physical arguments that are independent of any particular model of magnetic monopoles. It therefore makes an ideal monopole detector in the absence of an established theoretical understanding of monopole interactions. *The absence of a signal in an inductive detector provides incontrovertible evi-*

dence against the passage of monopoles through that detector and sets upper bounds on the particle flux which are very reliable.

III. THREE-LOOP DETECTOR

The three-loop detector was operated from January 1983 until March 1986. It consists of three mutually orthogonal superconducting loops shielded from external magnetic fluctuations by a superconducting shield. A fourth superconducting loop is present to provide a magnetic calibration signal. This section describes the apparatus in detail, including the configuration of the detector, calculations of the inductance between the detector loops and the calibration loop, use of coincidence information for spurious event discrimination, and the auxiliary equipment which provides further discrimination against spurious events.

A. Detector configuration

Fluctuations in the Earth's magnetic field are on the order of 10^{-4} G (about 10^{-4} of the Earth's field); the flux in an 81-cm^2 -area loop from these fluctuations is about five orders of magnitude greater than the monopole signal itself. We isolate the detector from external fields with two magnetic shields: a high-permeability (mumetal) room-temperature shield, which is continually degaussed, and an ultralow-field superconducting shield which uses an expanded-lead foil technique [47,48]. The ambient field in the detection region is ≈ 20 nG, and the combined shielding provides 160-dB attenuation of external magnetic-field variations.

To maximize the detector area and signal-to-noise ratio, we must make efficient use of the available detector volume. In one limit we could use very large detector loops, but they are then susceptible to external magnetic-field variations. Also, their high inductance would reduce the coupling to the SQUID and, therefore, the signal size. A further problem with large loops arises from the interaction of the shield and the loops, mentioned in the previous section. The detector loops couple to the magnetic field produced by the vortices at the points of entry and exit of the monopole, smearing the distribution of expected monopole signals. As a result, to maintain an acceptably large signal level and an acceptably small signal smearing, the loops cannot extend too close to the shield.

Operation of the original noncoincidence single-loop detector [27] demonstrated the need for discrimination against spurious events. Along with monitoring other known causes of spurious signals (discussed later), the most reliable technique is to use coincidence detection, having two or more uncoupled detectors that will respond in coincidence to a monopole event but not to a spurious event.

We designed the three-loop detector to achieve these goals. It is shown schematically in Fig. 3. Three loops are mounted orthogonally on the surface of a sphere as great circles, which inductively decouples them to first order. The loop radius is half the shield radius so that

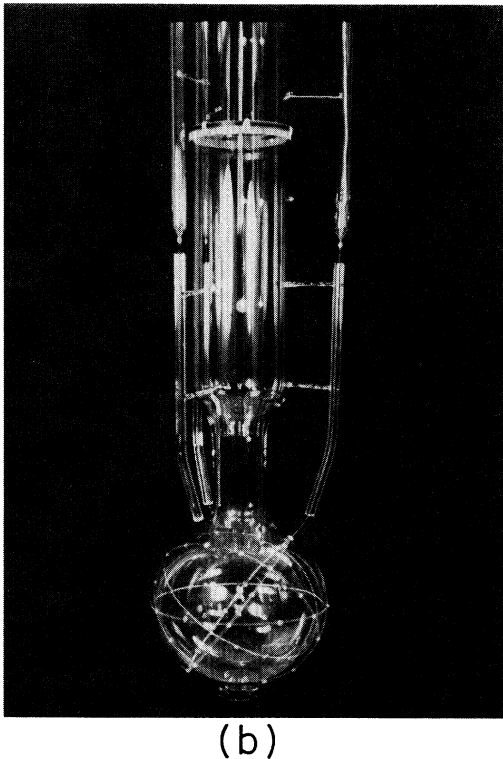
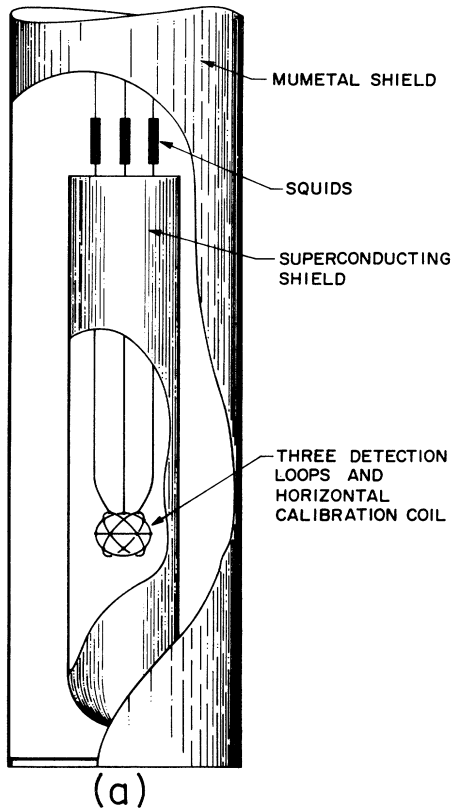


FIG. 3. (a) Schematic of three-loop detector. (b) Photo of three-loop assembly.

the loops are as large as possible while maintaining reasonable decoupling from the superconducting shield. Nevertheless, the coupling between the loops and shield is strong enough that monopole trajectories which miss the loops but intersect the superconducting shield could be detected. This effect increases the effective sensing area of the detector and provides some trajectory directionality. These points are discussed fully in a separate paper [49].

The detector is inside a cylindrical superconducting shield made of 63- μm -thick lead. The shield's radius is 10.16 cm and its length is 1 m. The bottom of the shield is closed, and the detector is 72 cm from the open top. The detector itself consists of the three mutually orthogonal loops wound on a spherical glass bulb. The bulb is 5.08 cm in radius, and each loop contains two turns of 0.013-cm-diameter niobium wire. The three loops are connected to independent SQUID magnetometers which monitor the currents. The passage of a Dirac charge through any loop of this detector would cause a $4\Phi_0$ flux change ($2\Phi_0$ for each turn). The (1,1,1) direction in a coordinate system whose axes are the three loop normals is coincident with the axis of the shield, and so the angle between the shield axis and each loop normal is $\theta = \arccos(1/\sqrt{3})$. A two-turn calibration loop with axis along the shield axis and concentric with the detector loops is also present.

B. Coincidence requirements

A detailed analysis for the response of the three-loop detector to the passage of magnetic charges has been published previously [49], and we only summarize the results here. With three loops we can dramatically increase our discrimination against spurious signals by requiring that an interesting signal must appear in coincidence in at least two of the three independent loop systems. In addition, as we discuss below, only certain combinations of signal values in the coincident loops would be consistent with the passage of a magnetic charge through the detector.

The three-axis geometry which we have chosen increases the probability of a monopole penetrating two or more loops. One can show that for our geometry of three mutually orthogonal loops lying on the surface of a sphere, the fraction of isotropic trajectories hitting the sphere and zero, one, two, or three loops is exactly $\frac{1}{8}$, $\frac{3}{8}$, $\frac{3}{8}$, and $\frac{1}{8}$, respectively. Thus $\frac{4}{7}$ of all trajectories hitting one loop will also hit at least one more.

Before discussing the detector response, it is important to remember the effect of the superconducting cylindrical shield around the loops. Although the passage of a Dirac charge through an isolated loop produces a current change given exactly by $4\Phi_0/L$ for our two-turn loops, where L is the self-inductance of the loop, this result is no longer true in the presence of the cylindrical shield. Now the passage of a monopole would also interact with the shield, leaving doubly quantized vortices at the entry and exit points through the shield. These newly appearing sources of magnetic flux also couple to the loop and modify the observed current change, almost always re-

ducing its magnitude. The signal now becomes dependent on the exact position of the trajectory entry and exit points and a distribution of possible signal sizes results, as shown in Fig. 4. We are also able to take advantage of trajectories which miss all three loops, but still penetrate the cylindrical shield. These trajectories are still observed by the loops if the entry or exit points are sufficiently close to the loops (Fig. 4).

Requiring double-coincident signals removes spurious signals caused, for example, by trapped flux motion within individual SQUID sensors and increases the discrimination of the detector against other spurious signals. This improvement is particularly dramatic for monopole trajectories which pass through at least one loop. Then as our calculations for the sensing-area distribution functions show [49], only certain combinations of signal sizes are possible for true monopole signals. We may characterize this effect by defining a three-dimensional phase space where each axis represents the current induced in each of the three loops. Several slices through this three-dimensional distribution function are shown in Fig. 5. If we consider the cubic volume contained within $\pm 4\Phi_0/L$ for each axis, then less than 1% of this volume corresponds to possible signal combinations resulting from a monopole which passes through at least one loop (Fig. 5). Likewise, for trajectories that miss all loops but still fall into the detectable near-miss category, double coincidence restricts the combinations of signals which can actually be caused by monopoles, but not by as large a factor (Fig. 5).

By utilizing the near-miss trajectories, the total sensing area of the detector is increased by a factor of 7 over the direct loop areas alone. However, in these cases the signal is small enough that without coincidence information a spurious signal in a single loop could be mistaken for a real one. Requiring double coincidence above a threshold magnitude of $0.1\Phi_0/L$ in all signals, including those that hit one or more loops, reduces the total sensing area of the detector by only 21% (from 601 to 476 cm^2), a reasonably small loss in sensing area considering the large increase in reliability.

A further requirement of simultaneous triple coincidence would reduce the total sensing area more than

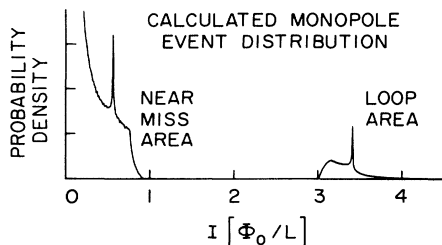


FIG. 4. Distribution of signal sizes observed in each loop from an isotropic distribution of monopole trajectories. Those signals above about $3\Phi_0/L$ correspond to trajectories passing through the loop, while those below about Φ_0/L correspond to trajectories which miss the loop, but penetrate the shield within about one diameter above or below the loop.

seems justifiable so that we decided on the double-coincident requirement. Only $\frac{1}{7}$ of all trajectories that intersect at least one loop also intersect all three, and the reduction in total sensing area, including the near-miss category, is 53% (from 601 to 280 cm^2). Such a stringent coincidence requirement would have been necessary only if a large number of spurious events were seen, which was not the case.

C. Auxiliary equipment

Certain auxiliary equipment connected to the detector provides information used to discriminate against spurious events. The most important of these is a single-axis accelerometer mounted on top of the Dewar with its

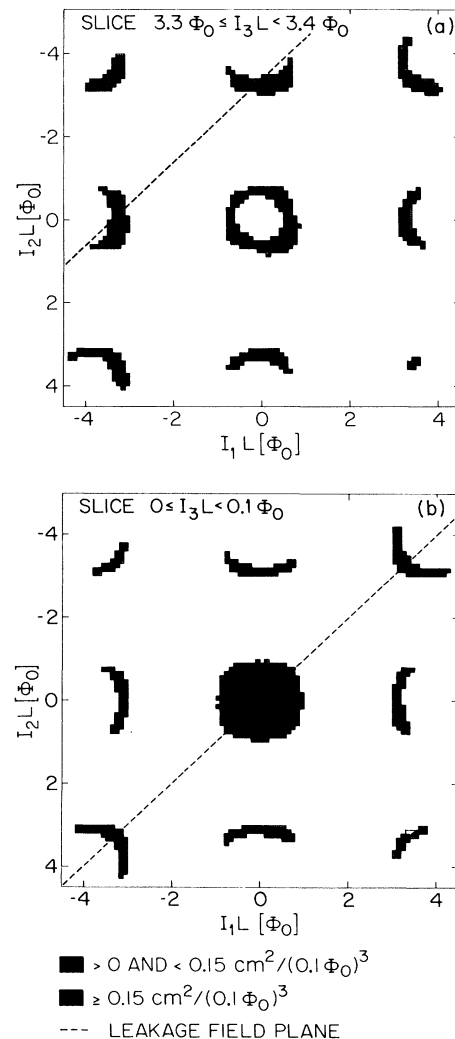


FIG. 5. Slices through three-dimensional distribution function for three-loop detector, showing the correlations between the signal sizes in the three loops for an isotropic flux of Dirac charge magnetic monopoles. Two slices are shown, and the dotted line represents the intersection of each plane with the plane of spurious signals caused by magnetic-field leakage.

sensing axis vertical. The computer samples the accelerometer output at high bandwidth (200 samples per second). The maximum absolute value of the high-bandwidth data in each 5-sec interval is stored on disk. Superconducting current offsets can be generated by tapping on the Dewar with a mallet, but these signals also show up clearly on the accelerometer data as shown in Fig. 6. We suspect these offsets are the result of motion of trapped flux in the SQUID's due to the acoustic wave pulse in the superconductors which make up the SQUID sensors [50] or the motion of the detector pickup loops in the ambient magnetic field; in any case, they are rarely larger than a few tenths of Φ_0 .

The motion of trapped flux from acoustic disturbances is also suspected as the cause for the single-channel offsets seen in the data (see Sec. VI). These acoustic disturbances originate from the occasional release of stresses stored in materials from thermal cycling. However, the disturbances which cause the single-channel offsets are localized within one of the SQUID sensors and are too weak to cause a signal in the accelerometer or to cause an offset in another SQUID sensor. These single-channel spurious offsets are removed from consideration by the coincidence requirement, since we have found that disturbances which cause offsets in more than one SQUID are always large enough to give an easily detectable accelerometer signal.

The computer also samples the output of a flux-gate magnetometer at 200 samples per second. Every 5 sec its output is averaged, and this average is stored on disk. The mumetal shield enclosing the detector apparatus is degaussed with a 60-Hz current to provide maximal shielding. We remove this 60-Hz signal from the magnetometer output with a 60-Hz notch filter. The magne-

tometer has been most helpful in rejecting those spurious events resulting from the detector's incomplete magnetic shielding, but all such events have been low-magnitude events. These events are usually caused by the motion of magnetized liquid-nitrogen cylinders or by trucks driving past the loading dock directly above the laboratory. External magnetic events are also identified by observing that the sum of the leakage fluxes induced in the three SQUID's is zero. This symmetry arises since any leakage field produces only horizontal field components \mathbf{B}_L near the center of the cylindrical shield [48] and since the sum of the three loop-area vectors \mathbf{A}_1 , \mathbf{A}_2 , and \mathbf{A}_3 is exactly vertical. Thus

$$\mathbf{B}_L \cdot \mathbf{A}_1 + \mathbf{B}_L \cdot \mathbf{A}_2 + \mathbf{B}_L \cdot \mathbf{A}_3 = \mathbf{B}_L \cdot (\mathbf{A}_1 + \mathbf{A}_2 + \mathbf{A}_3) = 0, \quad (2)$$

proving the result.

A cosmic-ray shower detector was in operation for 16 months from 6 September 1983 to 16 January 1985. During that time it detected, on average, one cosmic-ray shower per hour, and none of these events were found to correspond in any way to the five SQUID offsets that also occurred during that time. The cosmic-ray detector consisted of three scintillators measuring 15 cm \times 160 cm, each radiating from the Dewar to the corner of an equilateral triangle of side 185 cm centered at the Dewar. The Dewar is housed in a hole bored into a concrete plug 6 ft deep by 12 ft in diameter. The plug is mechanically separate from the rest of the laboratory structure, and the scintillators rested on top of this plug. The output pulse width of the discriminators was 50 nsec, and the pulses were fed to a logic unit that triggered on triple coincidences. The discriminator thresholds were set to detect about one triple coincident event per hour. On each triple coincidence, the logic unit produced a 50- μ sec output pulse, triggering a timer circuit that remained high for 8 sec. This signal was monitored every 5 sec by the computer. Subsequently, a more elaborate cosmic-ray detector was built around our detector apparatus by Peter Trower of Virginia Polytechnic Institute [51]. Its operation is reported in a separate paper by Trower.

An ultrasound motion detector and power line monitor are sampled every 5 sec by the computer. The motion detector is located just above the SQUID electronics. It is sensitive to motion within a radius of about 20 ft, an area which includes the detector, and it even detects the motion of the computer printer when operating. A power line monitor responds to power failure, low/high line voltage, voltage spikes, voltage drops, and high-frequency noise. Power line failures that do not affect computer operation are recorded by the computer. No coincidence has been found between the SQUID output and either the ultrasound motion detector or the power line monitor.

Changes in Dewar pressure can be a source of low-magnitude supercurrent offsets (output from the three SQUID's changes by an average of $\approx 0.05\Phi_0$ per millibar change in pressure). This correlation is easily seen in our data. In our laboratory the helium boil-off was collected in a building-wide recovery system. During most of the operation of the detector, the recovery system was not

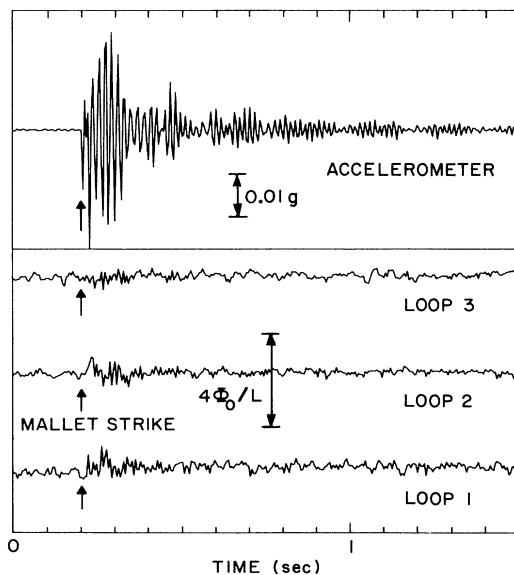


FIG. 6. Detector response to striking the detector with a mallet.

operational, but after it was repaired the Dewar was subject to frequent pressure changes because of activity in other laboratories. Attempts were made to isolate our Dewar from these pressure fluctuations by slightly pressurizing the Dewar and using a negative-feedback electronic circuit to maintain this constant pressure. However, as can be seen in Fig. 7(c), complete isolation was never obtained. Also, during liquid-helium transfers the circuitry had to be removed to allow the Dewar to vent and

was reconnected again after 12 h. We found that a spontaneous offset in one or more of the SQUID's would usually occur within 1–3 h of repressurizing, and so we eventually were forced to disconnect from the helium recovery system altogether (see Fig. 17).

When activities are occurring in the laboratory that are known to cause supercurrent offsets, such as liquid-nitrogen or -helium transfers into the Dewar, a veto flag is set in the computer to indicate that offsets during this time are not to be considered as monopole candidates. The data collector does not save high-bandwidth data (see Sec. V A) while this flag is set. Offsets found by the search algorithm are also discarded if the veto flag was set when they occurred.

IV. CALIBRATION-COIL COUPLING

The mutual inductance between the calibration loop and the detector loops determines the response to a current in the calibration loop. The superconducting shield affects the magnetic field produced by the calibration coil and is included in the calculation. We model the shield as N concentric superconducting loops with the restriction that the net flux in the shield is constant and does not change as the calibration current changes. The calculation has two parts; first, we calculate the current induced in the shield by the calibration current, and second, we calculate the flux through the detector loops produced by the current from the calibration loop and the induced currents from the shield.

We define the calibration loop radius a and the shield radius b . The induced current in the shield decays exponentially above and below the calibration loop, and so we need consider only a relatively small section of the shield near the loops. For convenience, we will consider the section within $\pm\pi b$ of the loops. The distance between each of the current loops making up the shield is then $d = 2\pi b / (N - 1)$. We restrict N to be odd and locate the calibration coil in the same plane as the loop identified as $(N + 1)/2$. Reserving the subscript 0 for the calibration loop and identifying each of the loops comprising the shield with subscripts 1– N , the following set of N linear equations describe the system:

$$\begin{aligned} -i_0 M_{01} &= i_1 L_1 + i_2 M_{12} + i_3 M_{13} + \dots, \\ -i_0 M_{02} &= i_1 M_{12} + i_2 L_2 + i_3 M_{13} + \dots, \\ -i_0 M_{03} &= i_1 M_{13} + i_2 M_{23} + i_3 L_3 + \dots, \\ &\dots, \end{aligned} \quad (3)$$

where $L_i = L$ is the self-inductance of each loop and M_{ij} is the mutual inductance between loop i and loop j . Each of these equations follows from the constraint that the flux change (current times inductance) in the shield is zero. This set of equations is not undetermined since the "variable" i_0 , the calibration current, is given.

In calculating the inductance matrix M_{ij} , we make use of inductance formulas found in Grover [52] and recognize that superconductors behave much like normal conductors at very high frequencies. The dc current in a superconducting wire flows within a penetration depth of

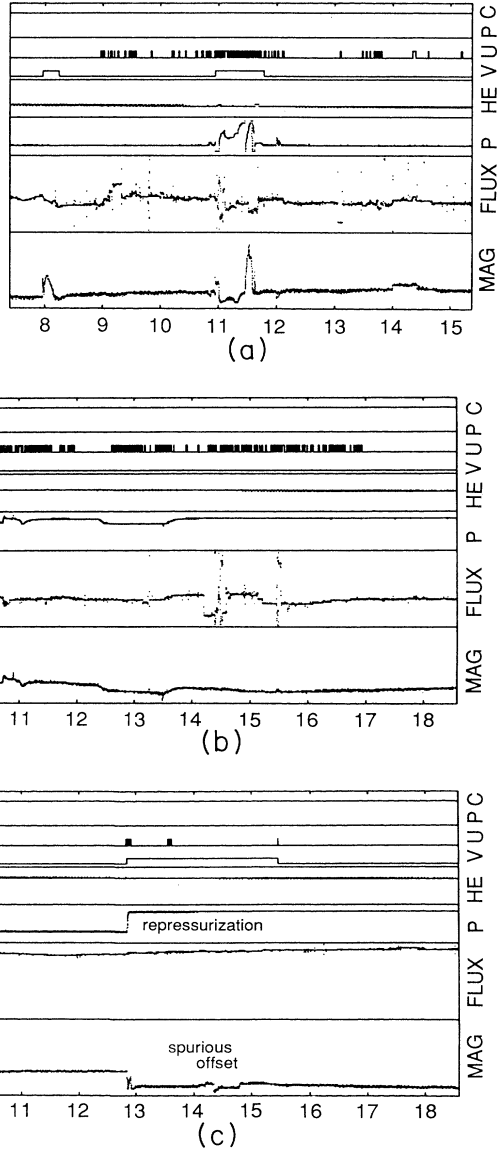


FIG. 7. (a) Typical pressure fluctuation after connecting to recovery system, but before pressure-isolation modifications (P is pressure; MAG is square root of sum of squares of SQUID signals). (b) Typical pressure fluctuation from recovery line after pressure-isolation modifications. (c) Spurious offset after repressurizing Dewar. Pressure was lowered to allow for liquid-helium transfer. Spurious offsets typically occurred 1–3 h after repressurization.

the surface, much like the high-frequency ac current in a normal conductor flows within the skin depth of the surface.

For a single shield loop, the self-inductance is that of a loop of radius b made of wire of diameter t (which we take to be the thickness of the shield):

$$L = \mu_0 b \left[\ln \left[16 \frac{b}{t} \right] - 2 \right]. \quad (4)$$

For other shield loops, the mutual inductance is that between concentric loops of radius b separated by a distance $x \neq 0$:

$$M_{ij} = M_{ji} = \frac{\mu_0 b}{k} [(2 - k^2)K(k) - 2E(k)], \quad (5)$$

where $k^2 = 4b^2 / (4b^2 + x^2)$ and $x = (j - i)d$ (i and j are the indices of the two loops). $K(k)$ and $E(k)$ are complete elliptic integrals of the first and second kinds, respectively. The mutual inductance between the calibration loop and shield loops is quite similar and given by

$$M_{0i} = \frac{\mu_0 \sqrt{ab}}{k} [(2 - k^2)K(k) - 2E(k)], \quad (6)$$

where now $k^2 = 4ab / [(a + b)^2 + x^2]$ and $x = d[(N + 1)/2 - i]$.

Given the matrix M_{ij} , Eq. (3) was solved numerically for various values of N to yield the current distribution induced in the shield as a function of the distance from the calibration coil plane. The results are plotted in Fig. 8.

The above calculation gives the effective mutual inductance between the calibration loop and shield; we now calculate the mutual inductance M between the calibration loop and detector loops. Given the flux Φ coupling to a detector loop induced by a current i_0 in the calibration coil, the mutual inductance is $M = \Phi / i_0$. The flux Φ is found from $\Phi = \oint \mathbf{A} \cdot d\mathbf{l}$, where $\mathbf{A} = \mathbf{A}_0 + \sum \mathbf{A}_j$ is the magnetic vector potential created by the current in the calibration loop and the current induced in the shield.

In cylindrical coordinates (r, θ, z) the vector potential of a current loop of radius a carrying current I is $\mathbf{A}_0 = A_0 \hat{\theta}$, where

$$A_0 = \frac{\mu_0 I}{2\pi} \left[\frac{a}{r} \right]^{1/2} f(k), \quad (7)$$

$$f(k) = [(2 - k^2)K(k) - 2E(k)] / k,$$

$$k^2 = \frac{4ar}{(a + r)^2 + (z - d)^2},$$

and the loop is located at $z = d$.

Therefore, the net vector potential induced by the current i_0 in the calibration loop is $\mathbf{A} = A \hat{\theta}$, where

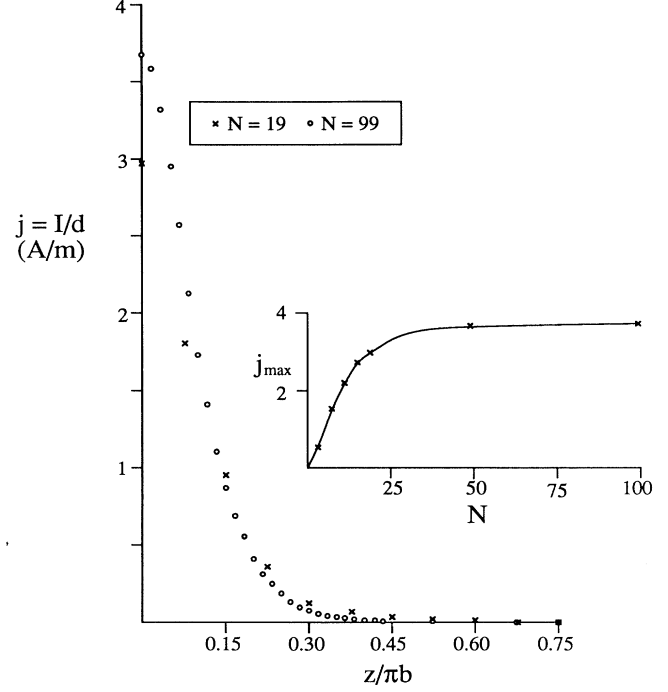


FIG. 8. Current density in superconducting shield as a function of distance from the calibration loop plane for a calibration current of 1 A, for $b = a/2$ and for $N = 19$ and 99. The inset shows the maximum value of the current density as a function of the number of loops N used in the calculation.

$$A = A(r, z) = \frac{\mu_0}{2\pi\sqrt{r}} \left[\sqrt{a} i_0 f(k_0) + \sum_{j=1}^N \sqrt{b} i_j f(k_j) \right], \quad (8)$$

$$k_0 = 4ar / [(a + r)^2 + z^2],$$

$$k_j = 4br / [(b + r)^2 + (z - d_j)^2],$$

$$d_j = d[(N + 1)/2 - j],$$

and i_j is the current in the shield found previously.

To perform the line integral along the tilted loop circuit, we now transform coordinates to the tilted plane defined in Fig. 9 where ψ is the azimuthal angle in the

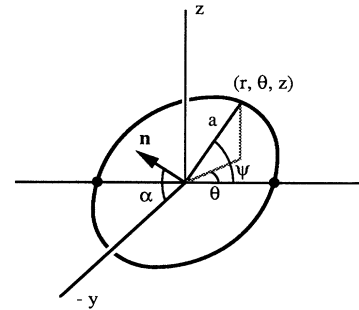


FIG. 9. Coordinate transformation to a tilted loop of radius a for the line integral.

loop plane. In this geometry, $\cos\alpha = \sqrt{1/3}$ and $\sin\alpha = \sqrt{2/3}$. Also, we can express the z and r coordinates in terms of ψ for each point along the tilted loop as $z = a \sin\alpha \sin\psi$ and $r = a(1 - \sin^2\alpha \sin^2\psi)^{1/2}$, where a is the loop radius and we use $z^2 + r^2 = a^2$. The line element is $d\mathbf{l} = a d\psi \hat{\psi} = dr \hat{r} + r d\theta \hat{\theta} + dz \hat{z}$, and so for computing $\mathbf{A} \cdot d\mathbf{l}$ we need only the term $\hat{\theta} \cdot d\mathbf{l} = r d\theta = (a^2 d\psi^2 - dr^2 - dz^2)^{1/2}$, since \mathbf{A} is purely along $\hat{\theta}$. Also, we use the element $dr = -a \sin^2\alpha \sin\psi \cos\psi d\psi / (1 - \sin^2\alpha \sin^2\psi)^{1/2}$ and the element $dz = a \sin\alpha \cos\psi d\psi$. Thus we obtain

$$r d\theta = a d\psi \left[\frac{1 - \sin^2\alpha}{1 - \sin^2\alpha \sin^2\psi} \right]^{1/2} = d\psi \frac{a^2 \cos\alpha}{r}. \quad (9)$$

Therefore, since the total flux Φ coupling to the tilted loop from a current i_0 in the calibration coil is given by $\Phi = \int \mathbf{A} \cdot d\mathbf{l}$, we finally obtain the mutual inductance as

$$M = \frac{\Phi}{i_0} = \frac{a^2 \cos\alpha}{i_0} \int_0^{2\pi} \frac{A(r(\psi), z(\psi)) d\psi}{r(\psi)}, \quad (10)$$

which completes the algebraic calculation.

Equation (10) can be integrated numerically if care is taken to avoid the singularities at $\psi=0$ and π which occur for the elliptic integrals $K(k)$ and $E(k)$ at $k=1$. The integrations were performed using trapezoidal integration with Romberg corrections. The sensitivity of the mutual inductance to the geometric uncertainties in the shield was studied by adjusting a through several percent. This adjustment resulted in changes of less than 1%. In addition, the convergence of the line integral was tested by doubling the number of points from 64 to 128. The difference between the values of M calculated with 64 and 128 points was less than 2%.

Figure 10 shows the results of the calculated M for various numbers of loops used to approximate the shield. The case $N=0$ defines the mutual inductance between the calibration and detector loops in the absence of the shield. We see that the shield decreases the mutual inductance by about 13% and that the asymptotic value has been reached at about 49 loops. Since this result is for single-turn calibration and detector loops and both

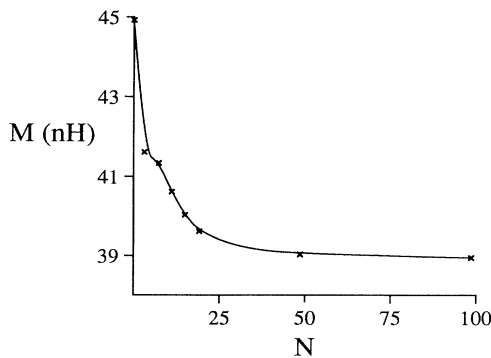


FIG. 10. Net mutual inductance between calibration loop and detector loop as a function of N , the number of loops approximating the shield.

loops have two turns, the actual value of M is 2×2 or 4 times this value. The final value is 155.6 nH, so that a current of 53.2 nA ($4\Phi_0/155.6$ nH) will induce a supercurrent change of $\pm 4\Phi_0/L$ in each loop.

V. DIGITAL DATA-COLLECTION SYSTEM

A Digital Equipment PDP-11/23 simultaneously acquires data at 200 samples per second in five channels through a 12-bit analog-to-digital converter. By running the collector as an uninterruptible batch job on a multi-tasking operating system (RSX V4.1), all but a few percent of the computer CPU time remains available for interactive data analysis and detector modeling during detector operation. The data-collection program stores its data in a double buffer. As the buffers fill, their data are filtered to reduce bandwidth and stored to disk. Each buffer occupies about 20 bytes (4 kbytes per channel or 2000 samples per buffer). The total load on the computer from the data-collection and filter routines is roughly 20% in both execution time and memory. Every 40 filtered samples, the system time and other collector parameters are stored to maintain data integrity. Also, as the collector and filter routines run they write pertinent time-stamped status information, such as the detection of events or missed interrupts, to the system log file. Figure 11(a) summarizes the data-collection system.

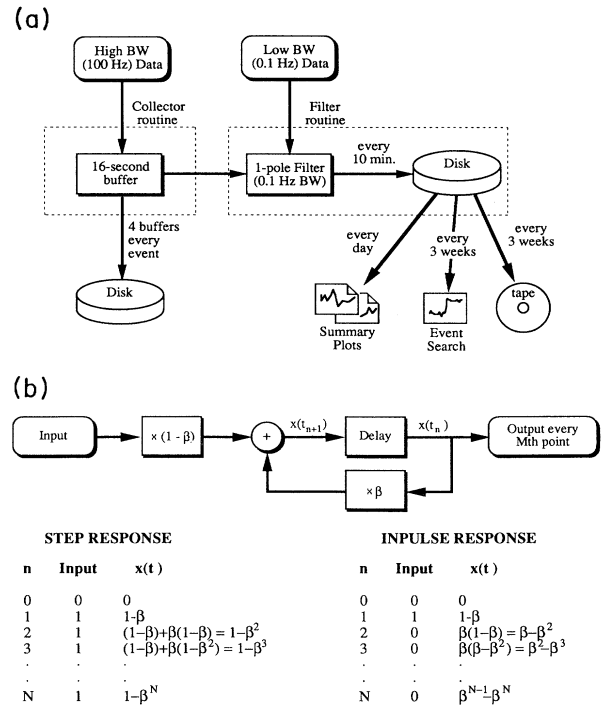


FIG. 11. (a) Block diagram of data-collection system. (b) Schematic diagram of digital filter, showing step and impulse responses. This algorithm produces a single-pole low-pass filter at a frequency ν for a sampling rate R , where $\beta = e^{-2\pi\nu/R}$. We use $\nu = 0.1$ Hz, $R = 200$ points/sec, and keep every M th point using the Nyquist criterion $M = R/(2\nu) = 1000$.

A. Filtering and storage

Five channels of data are collected at a bandwidth of 100 Hz (200 samples per second): the output of the three SQUID's, the accelerometer, and the external flux gate magnetometer. The SQUID data come directly from the SQUID electronics, which include output 100-Hz low-pass filters. This signal is monitored both by a strip-chart recorder through an electronic 0.1-Hz bandwidth filter and by the computer through a 12-bit analog-to-digital converter. The computer processes these data using a digital 0.1-Hz single-pole low-pass filter (one output point every 5 sec). A block diagram of the digital filter is shown in Fig. 11(b), which also illustrates the exponentially decaying response of the filter to a step function. The accelerometer bandwidth is reduced to 0.1 Hz by finding the maximum absolute value of its output during the filter cycle. The magnetometer output is likewise reduced to 0.1 Hz by a simple average. Several data are collected by the computer at 0.1-Hz bandwidth (one sample every 5 sec): output from the ultrasound detector, the power line monitor, the cosmic-ray detector, the "veto" line, and the helium level and Dewar pressure. This information is all stored to disk on a regular basis and then later backed up to tape for archival storage.

As the filter processes the data, it checks the filtered SQUID output for offsets larger than a preset threshold (usually $0.1\Phi_0/L$) by comparing the current filtered value to the previous. If an offset is found, then a message is sent to the data-collection routine causing it to store the high-bandwidth data to disk. The high-bandwidth data is stored by immediately saving the oldest buffer in the double-buffer structure and then alternately saving each of the two buffers as they fill, until a total of eight buffers worth of data are saved. This provides about 5 sec of high-bandwidth data before the event (on average) and about 1 min after the event. These data are then used to check for coincidence between the SQUID's, accelerometer, and magnetometer outputs. However, the noise level in the high-bandwidth data often mask any coincidences. The filtered data generally provide a more useful means of checking for coincidences.

B. Data summaries

The filtered data is automatically plotted by the computer each night to give three 8-h summaries of the collector operation. These reports are each two pages long with the SQUID and accelerometer outputs on one page and the SQUID magnitude (square root of sum of square of the three loops), magnetometer, and low-bandwidth data on the other. A typical data summary is shown in Fig. 12. These often provide all the information needed to distinguish the causes of spurious events or to alert us to detector performance problems such as an increase in noise levels or faulty electronics. A program which plots the data at higher resolution is also available in case additional information is needed.

When an event causes high-bandwidth data to be saved to disk, these are plotted in a summary plot that includes all five high-bandwidth channels on a single page. An ex-

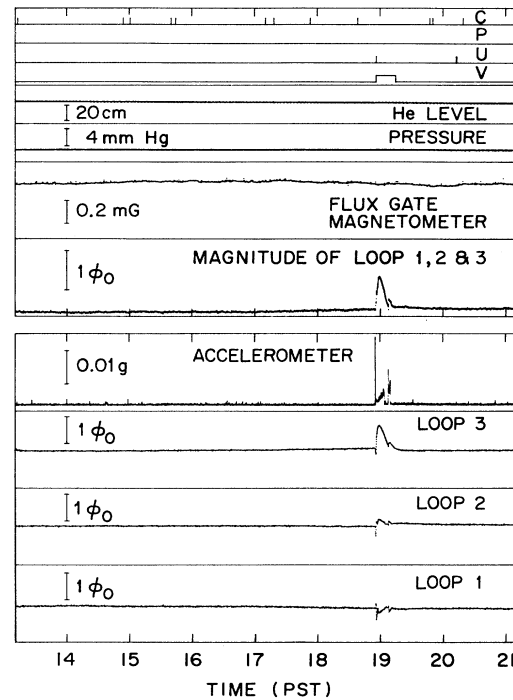


FIG. 12. Typical data summaries of the filtered data from the three-loop detector, produced on a daily basis.

ample of this output is shown in Fig. 13. If more detailed information is needed, a program is available that allows one to view any portion of the data at various magnifications.

C. Identifying events

On a periodic basis the filtered SQUID data are searched by a computer for offsets greater than $0.1\Phi_0$. Since this does not need to be done in real time a look-

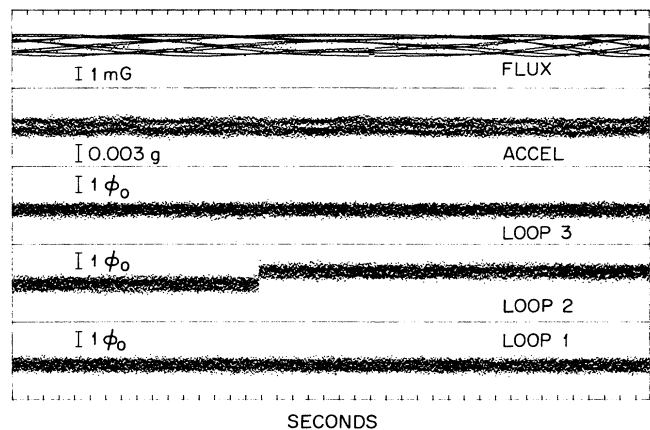


FIG. 13. Typical data summary of the unfiltered data from the three-loop detector, produced after each event. This one shows a typical single-channel unexplained offset.

ahead technique to detect events is possible. When a monopole crosses the detector, the flux changes much more rapidly than 0.1 Hz, providing a step-function input to the data collector. The digital filter causes the output to rise to its maximum value according to its $1/RC$ time constant. It reaches about 90% of its maximum value in 5 sec (one sample) and 99% in 10 sec (two samples), and so at most two data points will pass before the output has essentially reached maximum. On the other hand, the rise time is fast enough that offsets can be detected by simply examining adjacent samples.

Once an offset above threshold is detected, the previous 8 min of data (100 data points) are checked for excessive noise or slow ramps by comparing the largest difference between the first value and the following 99 samples to the threshold. This 8 min of data are then averaged, two samples are skipped to allow for rise time, and a similar analysis is made on the following 8 min. These two averages are compared, and if both sets of data are free of excessive noise and the difference between the averages is above threshold, then an event is reported.

This procedure was necessary in order to avoid detecting liquid-nitrogen transfers as offsets. During a liquid-nitrogen transfer, the Dewar-neck temperature profile changes rapidly and mechanical motion of the detector assembly occurs, resulting in large SQUID output excursions. The SQUID response is usually consistent, however, showing a large initial signal drop of about $-0.5\Phi_0$ followed by a rapid rise of about $1\Phi_0$, which then slowly decays over 15 min back to the previous equilibrium value. By comparing differences between samples in an 8-min buffer, large excursions are detected, such as the one shown in Fig. 14(a), and by comparing the largest difference between the first value and all others slow decay or drift is detected, such as the case shown in Fig. 14(b). Finally, comparing averages over these 8-min segments gives an accurate value of the offset size.

Active operation time is determined by counting only that time when all three SQUID's are quiet. If any of the three SQUID's show an offset which is later rejected by the search algorithm, that time is deducted from the ac-

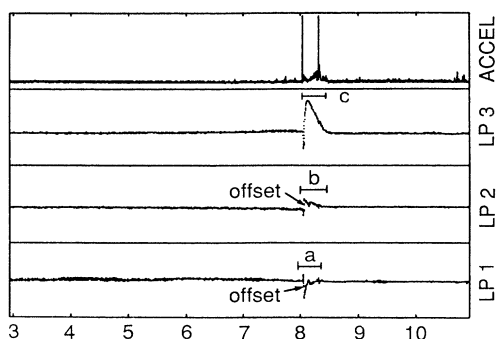


FIG. 14. Example of filtered data offsets that will be rejected by the search algorithm because of (a) noisy data before or after the offset or (b) drift in the data before or after the offset; (c) rises too slowly to be detected as an offset.

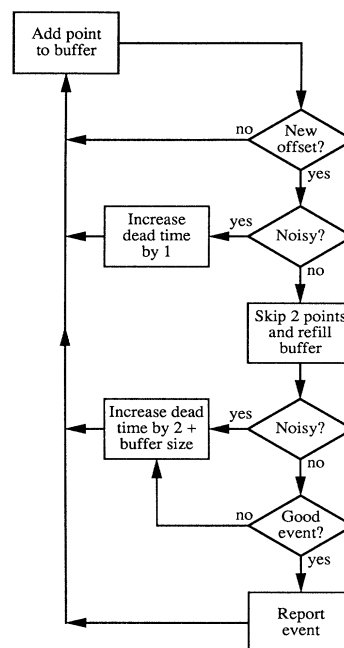


FIG. 15. Flow chart of algorithm to search for events in the filtered data. Execution begins in box at top left until the buffer has filled and proceeds through the loop until the end of the file is reached. Live time is determined by the total number of points in a file less the number of dead points. See text for definitions of offsets, noise, and events.

tive detector-operation time. A flow diagram of the search algorithm is shown in Fig. 15 (the PASCAL code is included in an appendix of Ref. [53]).

One problem encountered while programming related to crossing file boundaries during a search. The difficulty occurs because the data-collection routines store the filtered data in interleaved blocks; i.e., it stores 50 channel-1 values followed by 50 channel-2 values followed by 50 channel-3 values, etc., then skips some space to reach a disk block boundary, and starts over. The look-ahead nature of the algorithm (which occurs only when offsets are detected) then causes the program to reach the end of the file for one loop before it does for the others. This made it necessary for the algorithm to be written so that it scanned the file 3 times, once for each detector loop; coercing this scheme into crossing file boundaries proved too difficult. It was therefore necessary to unconditionally throw out the first and the last buffers (100 points). The result is that about 3% of the data is thrown out without ever being examined or included in the active detector operation time. This loss of data seemed minor compared to the effort that would have been necessary to correct the problem.

VI. DETECTOR OPERATION AND CONCLUSIONS

The three-loop detector, at 476 cm^2 averaging sensing area (74 cm^2 of direct sensing area and 402 cm^2 of near-miss area through the shield), was in operation from 25

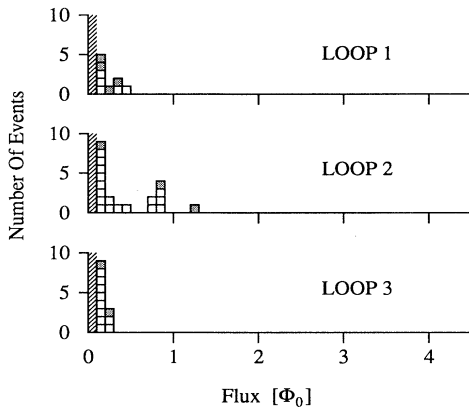


FIG. 16. Histogram of events above threshold prior to elimination by coincidence veto. Shaded events occurred during the first 5 days of operation.

January 1983 to 20 March 1986, until it was shut down to provide parts for the larger eight-channel detector now being operated at Stanford. During that time, the detector logged 24 190 h of active operation.

We observed a total of 41 unexplained events, 9 of which occurred in the first 5 days of operation during a settling period of generally noisy data. A histogram of all unexplained events is shown in Fig. 16. Offsets from known causes are not included. No vetoes based exclusively on the accelerometer data have been necessary. None of the unexplained events satisfy the double-coincidence requirement, removing all from consideration as monopole candidates. If we assume the events are uncorrelated, after the first 5 days of operation, there were 32 spurious offsets during 8.7×10^6 intervals each 10 sec wide. The corresponding accidental double-coincidence rate is $(32/8.7 \times 10^6)^2$ per window or about one every 25 000 yr. As Fig. 17 shows, the accidental double-coincidence rate during several periods of operation, such as January 1984 through January 1985, was significantly lower (once every 3×10^6 yr).

Most vetoed offsets were due to mechanical, external magnetic, or electrical causes and were below $0.5\Phi_0$. None of the unexplained events were large and none were

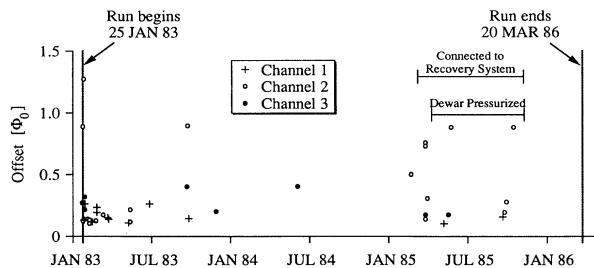


FIG. 17 Time plot of unexplained events above threshold prior to elimination by coincidence veto.

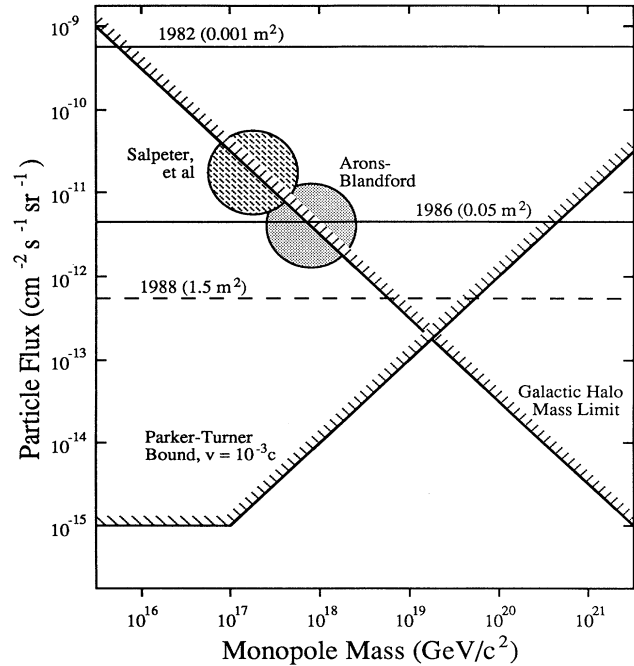


FIG. 18. Flux limit from three-loop detector search for magnetic monopoles. The astrophysical limits discussed in Sec. IA are shown as well as the new limit set by the Stanford eight-channel detector (see accompanying paper).

coincident. Thus these data cast no new light on the origin of the candidate reported by Cabrera in 1982 [27]. However, these data lower that flux limit by a factor of 319, substantially increasing the probability of a spurious cause for that event. With no candidate events, these data set an upper limit of $4.4 \times 10^{-12} \text{ cm}^{-2} \text{ sr}^{-1} \text{ sec}^{-1}$ at 90% C.L. ($2.3/\int dA d\Omega dt$) on any uniform flux of magnetic monopoles of any mass passing through the Earth's surface at any velocity.

The relation of these data to our previous experiment is summarized in Fig. 18, with the Parker and galactic-halo-mass bounds shown shaded (see also more recent paper on larger eight-channel detector [32]). The Arons-Blandford [12] and Salpeter-Shapiro-Wasserman [13] bounds (see Introduction) are shown as shaded circles.

As more complex grand unified theories push the monopole mass toward the Planck mass at $10^{19} \text{ GeV}/c^2$ and the with the Farouki-Shapiro-Wasserman [14] corrections to the Parker bound, mass-independent monopole searches are approaching limits that are of current theoretical interest.

ACKNOWLEDGMENTS

We wish to thank J. Bourg for setting up and programming the data-acquisition computer and R. Huckaby for constructing the Pyrex coil form assembly. This work has been funded in part by DOE Contract No. DE-AM03-76SF00-326 and by an equipment supplement from NSF Grant No. DMR 80-26007.

- *Present address: Department of Physics, C.B. 172, University of Colorado at Denver, P.O. Box 173364, Denver, CO 80217-3364.
- [1] P. A. M. Dirac, Proc. R. Soc. London **A133**, 60 (1931); Phys. Rev. **74**, 817 (1948); Int. J. Theor. Phys. **17**, 235 (1978).
 - [2] G. 't Hooft, Nucl. Phys. **B79**, 276 (1974).
 - [3] A. M. Polyakov, Pis'ma Zh. Eksp. Teor. Fiz. **20**, 430 (1974) [JETP Lett. **20**, 194 (1974)].
 - [4] J. Preskill, Annu. Rev. Nucl. Part. Sci. **34**, 461 (1984).
 - [5] D. E. Groom, Phys. Rep. **140**, 325 (1986).
 - [6] *Monopole '83*, Proceedings of the NATO Advanced Study Institute, Ann Arbor, Michigan, 1983, edited by J. L. Stone, NATO ASI, Series B: Physics Vol. III (Plenum, New York, 1984).
 - [7] H. J. Fritsch, in *Monopole '83* (Ref. 6), p. 515, presents an excellent review of inductive detectors.
 - [8] *Magnetic Monopoles*, edited by R. A. Carrigan and W. P. Tower (Plenum, New York, 1983).
 - [9] E. N. Parker, Astrophys. J. **122**, 293 (1955); **160**, 383 (1970); E. N. Parker, *Cosmical Magnetic Fields* (Clarendon, Oxford, 1979).
 - [10] M. S. Turner, E. N. Parker, and T. J. Bogdan, Phys. Rev. D **26**, 1296 (1982).
 - [11] E. N. Parker, in *Monopole '83* (Ref. 6), p. 125.
 - [12] J. Arons and R. D. Blanford, Phys. Rev. Lett. **50**, 544 (1983).
 - [13] E. E. Salpeter, S. L. Shapiro, and I. Wasserman, Phys. Rev. Lett. **49**, 1114 (1982).
 - [14] R. Farouki, S. L. Shapiro, and I. Wasserman, Astrophys. J. **284**, 282 (1984); D. Chernoff, S. L. Shapiro, and I. Wasserman, *ibid.* **304**, 799 (1986).
 - [15] C. R. Dokos and T. N. Tomaras, Phys. Rev. D **21**, 2940 (1980).
 - [16] V. A. Rubakov, Pis'ma Zh. Eksp. Teor. Fiz. **33**, 658 (1981) [JETP Lett. **33**, 644 (1981)]; V. A. Rubakov, Nucl. Phys. **B203**, 311 (1982); V. A. Rubakov and M. S. Serbryakov, *ibid.* **B218**, 240 (1983).
 - [17] C. G. Callan, Phys. Rev. D **25**, 2141 (1982); **26**, 2058 (1982).
 - [18] D. P. Bennett, Phys. Rev. D **31**, 2323 (1985).
 - [19] S. D. Drell, N. M. Kroll, M. T. Mueller, S. J. Parke, and M. A. Ruderman, Phys. Rev. Lett. **50**, 644 (1983).
 - [20] N. M. Kroll, S. J. Parke, V. Ganapathi, and S. D. Drell, in *Monopole '83* (Ref. 6), p. 295.
 - [21] N. M. Kroll and V. Ganapathi, in *Resonance Ionization Spectroscopy and Its Application, 1984*, Proceedings of the Second International Symposium, Knoxville, Tennessee, 1984, edited by G. S. Hurst and M. G. Payne, IOP Conf. Proc No. 71 (IOP, London, 1984).
 - [22] L. W. Alvarez, Lawrence Berkeley Lab. Physics Note No. 470, 1963 (unpublished).
 - [23] L. J. Tassie, Nuovo Cimento **38**, 1935 (1965).
 - [24] P. Eberhard, Lawrence Berkeley Lab. Physics Note 506, 1964 (unpublished).
 - [25] P. Eberhard, D. Ross, L. Alvarez, and R. Watt, Phys. Rev. D **4**, 3260 (1971).
 - [26] R. R. Ross, P. H. Eberhard, L. W. Alvarez, and R. D. Watt, Phys. Rev. D **8**, 689 (1973).
 - [27] B. Cabrera, Phys. Rev. Lett. **48**, 1378 (1982).
 - [28] B. Cabrera, M. Taber, R. Gardner, and J. Bourg, Phys. Rev. Lett. **51**, 1933 (1983).
 - [29] B. Cabrera, M. Taber, R. Gardner, M. Huber, and J. Bourg, in *Monopole '83* (Ref. 6), p. 439.
 - [30] R. Gardner, B. Cabrera, M. Taber, and M. Huber, in *LT-17*, Proceedings of the Seventeenth International Conference on Low Temperature Physics, Karlsruhe, West Germany, 1984, edited by U. Eckern, A. Schmid, W. Weber, and H. Wuehl [Physica **126B&C** (1-3), 945 (1984)].
 - [31] M. Taber, B. Cabrera, R. Gardner, and M. Huber, in *Inner Space/Outer Space: The Interface Between Cosmology and Particle Physics*, Proceedings, Batavia, Illinois, 1984, edited by R. W. Kolb *et al.* (Univ. of Chicago Press, Chicago, 1986), p. 426.
 - [32] M. E. Huber, B. Cabrera, M. A. Taber, and R. D. Gardner, Phys. Rev. Lett. **64**, 835 (1990); see also M. E. Huber, B. Cabrera, M. A. Taber, and R. D. Gardner, following paper, Phys. Rev. D **44**, 636 (1991).
 - [33] C. D. Tesche, C. C. Chi, C. C. Tsuei, and P. Chaudhari, Appl. Phys. Lett. **43**, 384 (1983).
 - [34] C. C. Chi, C. D. Tesche, C. C. Tsuei, P. Chaudhari, and S. Bermon, in *Monopole '83* (Ref. 6), p. 451.
 - [35] S. Bermon, P. Chaudhari, C. C. Chi, C. D. Tesche, and C. C. Tsuei, Phys. Rev. Lett. **55**, 1850 (1985).
 - [36] S. Bermon, C. C. Chi, C. C. Tsuei, J. R. Rozen, P. Chaudhari, M. W. McElfresh, and A. Prodel, Phys. Rev. Lett. **64**, 839 (1990).
 - [37] J. R. Incandela, M. Campbell, H. Frisch, S. Somalwar, M. Kuchnir, and H. R. Gustafson, in *Monopole '83* (Ref. 6), p. 461.
 - [38] J. R. Incandela, M. Campbell, H. Frisch, S. Somalwar, M. Kuchnir, and H. R. Gustafson, Phys. Rev. Lett. **53**, 2067 (1984).
 - [39] S. Somalwar, H. Frisch, J. Incandela, and M. Kuchnir, Nucl. Instrum. Methods **226**, 341 (1984).
 - [40] J. C. Schouten, A. D. Caplin, C. N. Guy, M. Hardiman, and J. G. Park, in *Monopole '83* (Ref. 6), p. 471.
 - [41] C. N. Guy, in *Monopole '83* (Ref. 6), p. 491.
 - [42] A. D. Caplin, C. N. Guy, M. Hardiman, J. G. Park, and J. C. Schouten, Nature **317**, 234 (1985).
 - [43] T. Ebisu and T. Watanabe, J. Phys. Soc. Jpn. **52**, 2617 (1983); in *Monopole '83* (Ref. 6), p. 503; Phys. Rev. D **36**, 3359 (1987).
 - [44] Y. H. Kao, W. J. Yeh, and B. Y. Shi (unpublished).
 - [45] F. R. Fickett, M. Cromar, and A. F. Clark, in *Monopole '83* (Ref. 6), p. 477; A. F. Clark, M. Cromar, and F. R. Fickett, IEEE Trans. Magn. **MAG-21**, 418 (1985).
 - [46] See, for example, B. Cabrera, C. E. Cunningham, and D. Saroff, Phys. Rev. Lett. **62**, 2040 (1989).
 - [47] B. Cabrera, in *Magnetic Monopoles* (Ref. 8), p. 175.
 - [48] B. Cabrera, in *Near Zero*, edited by J. D. Fairbank, B. S. Deaver, C. W. F. Everitt, and P. F. Michelson (Freeman, San Francisco, 1988); pp. 312-322; B. Cabrera, Ph.D. thesis, Stanford University, 1975.
 - [49] B. Cabrera, R. Gardner, and R. King, Phys. Rev. D **31**, 2199 (1985).
 - [50] B. Cabrera, in *Principles and Applications of Superconducting Quantum Interference Devices*, edited by A. Barone (World Scientific, Singapore, in press).
 - [51] W. P. Trower (unpublished); see also W. P. Trower, in *Monopole '83* (Ref. 6), p. 625.
 - [52] F. W. Grover, *Inductance Calculations: Working Formulas and Tables* (Dover, New York, 1962).
 - [53] R. D. Gardner, Ph.D. thesis, Stanford University, 1987.

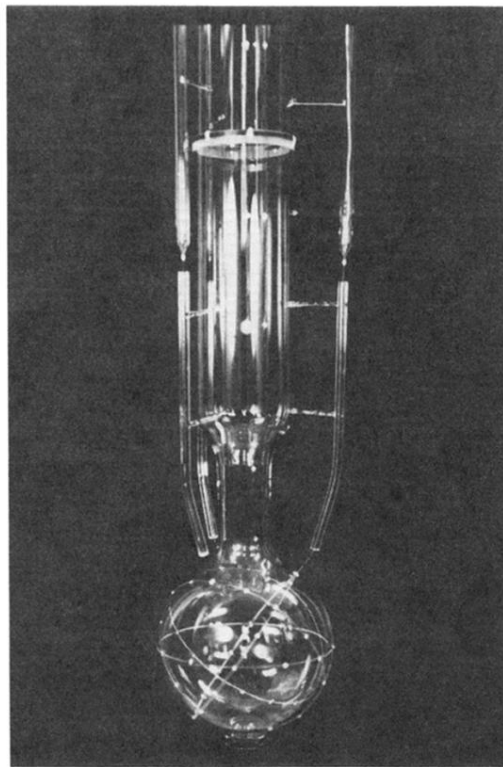
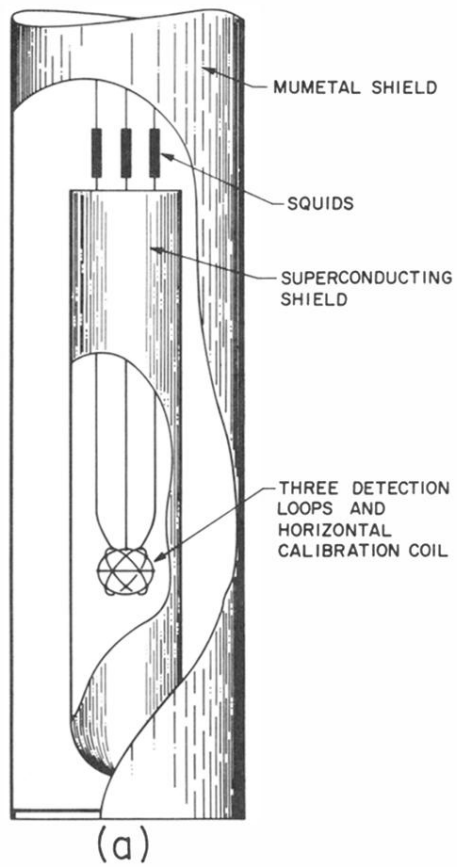


FIG. 3. (a) Schematic of three-loop detector. (b) Photo of three-loop assembly.